

# WIDE RANGE MULTI-PHASE RESONANT CONVERTERS

Bryce Hesterman  
Colorado Power Electronics, Inc.  
Fort Collins, Colorado

## ABSTRACT

Multi-phase resonant converters can operate efficiently at full output power over both a wide input voltage range and a wide output voltage range. They also provide additional significant advantages when compared to conventional converter topologies. The wide operating range allows considerable flexibility in how a given converter is used. Multi-phase resonant converters produce continuous power flow in contrast with the pulsating power flow that occurs in pulse-width modulated or pulse-rate modulated converters, consequently considerably less filtering capacitance is required for both the input and the output. Zero-voltage switching provides low switching losses, while low conduction losses are provided by a phenomenon that can be compared to a continuously-variable transmission in which rms currents in the switching transistors and transformers remain relatively constant over the full-power operating ranges of the input and output voltages. A novel output rectifier circuit is shown to enhance the wide-range capabilities of multi-phase resonant converters. The power flow of these wide-range converters is controlled by varying the switching frequency. The converters inherently provide short-circuit protection by limiting the switching currents and output currents occurring with a shorted output at any switching frequency in the operating range. The probability of having damaging single-event effects is reduced in comparison with other converter topologies because the voltages across the switching transistors do not exceed the dc input voltage, and voltages across the output rectifier diodes do not exceed the dc output voltage.

## INTRODUCTION

Resonant converters have been investigated as candidates for space applications, and particularly for electric propulsion<sup>1-4</sup>. Resonant converters have high efficiency, low mass and reduced sensitivity to single event burnout. Square wave converters are commonly specified to deliver full output power at the maximum output voltage. In contrast, resonant power converters are commonly able to deliver full output power over a 2:1 output voltage range<sup>4</sup>. Special output rectifier circuits have been developed that allow resonant converters to deliver full power over a 5:1 output voltage range<sup>5,6</sup>. This is graphically illustrated in Figure 1.

A Hall thruster power processing unit (PPU) prototype having a wide range resonant discharge supply has been developed by Colorado Power Electronics (CPE) for the NASA Glenn Research Center<sup>7,8</sup> using wide range resonant converter technology previously developed at CPE under internal funding<sup>6</sup>. The CPE wide range discharge supply provides full power over an output voltage range of 200 V to 700 V, which is a wide enough range for the intended application. Operation at 200 V output allows the development of high thrust for maneuvering, while high Isp can be produced by operating at higher output voltages. The CPE Hall thruster prototype PPU operates from an unregulated dc input bus that ranges from 80 V to 160 V. It uses resonant converters having 2:1 full-power output voltage ranges for the magnet, heater and keeper supplies. This paper briefly discusses the CPE Hall thruster prototype PPU. The standard and wide range resonant converters developed by CPE are compared, and single event effects are discussed.

DISTRIBUTION STATEMENT: Approved for public release; distribution is unlimited

Partially funded through NASA contracts NNC07CA12C and NNX10CD05P.

© Colorado Power Electronics, Inc. 2010.

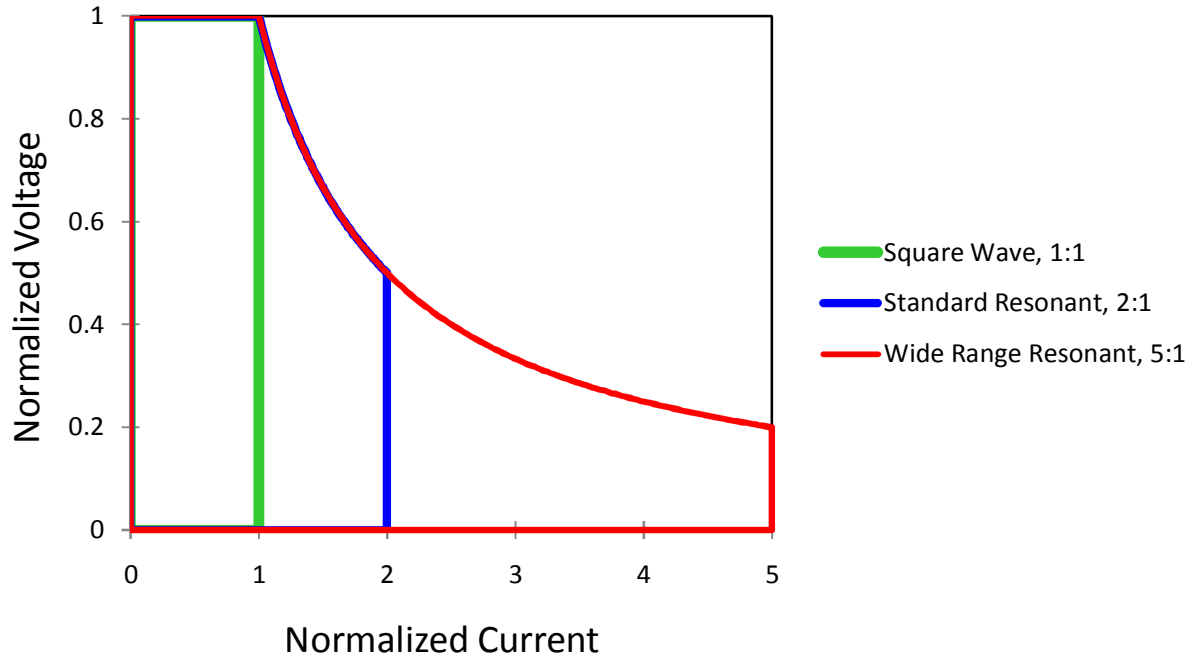


Figure 1. Normalized full-power output operating ranges for some square-wave and resonant converters.

## RESULTS AND DISCUSSION

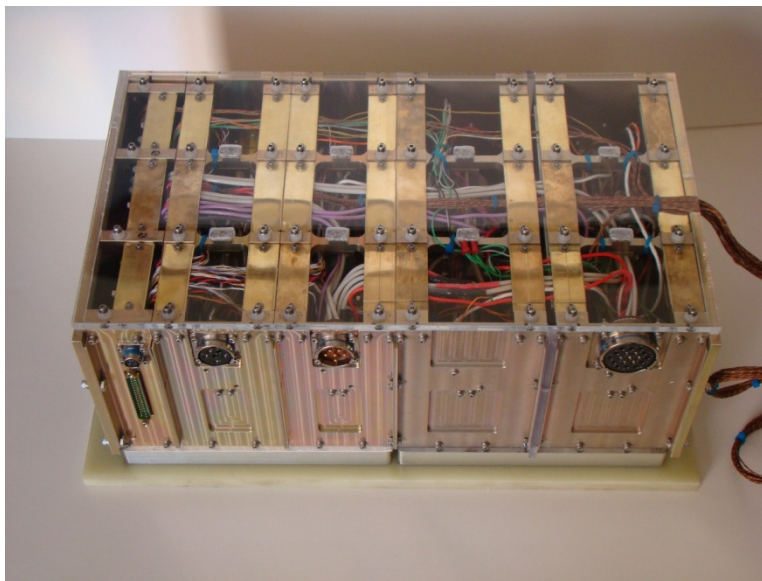


Figure 2. CPE Hall thruster PPU prototype.

Figure 2 shows the CPE Hall thruster PPU prototype. It has five modules. From left to right: Interface and housekeeping supply, Dual magnet supply, Heater and Keeper/Ignition supplies, Discharge master supply and Discharge slave supply. The supply voltages and currents are listed in Table 1.

Table 1. Wide Range PPU Operating Voltages, Currents and Power Levels.

Supply	Output Voltage, VDC	Output Current, A	Output Power, W
Ignition/Keeper	5 to 40	2.5 @ 40V 5 @ 20V	100
Heater	1 to 20	10 @ 20V 20 @ 10V	200
Dual Magnet (Per Supply)	5 to 40	5 @ 40 V 10 @ 20 V	200
Discharge (Per Supply)	200 to 700	2.68 @ 700V 10 @ 200V	2000

### STANDARD THREE-PHASE LCC SERIES-RESONANT CONVERTER

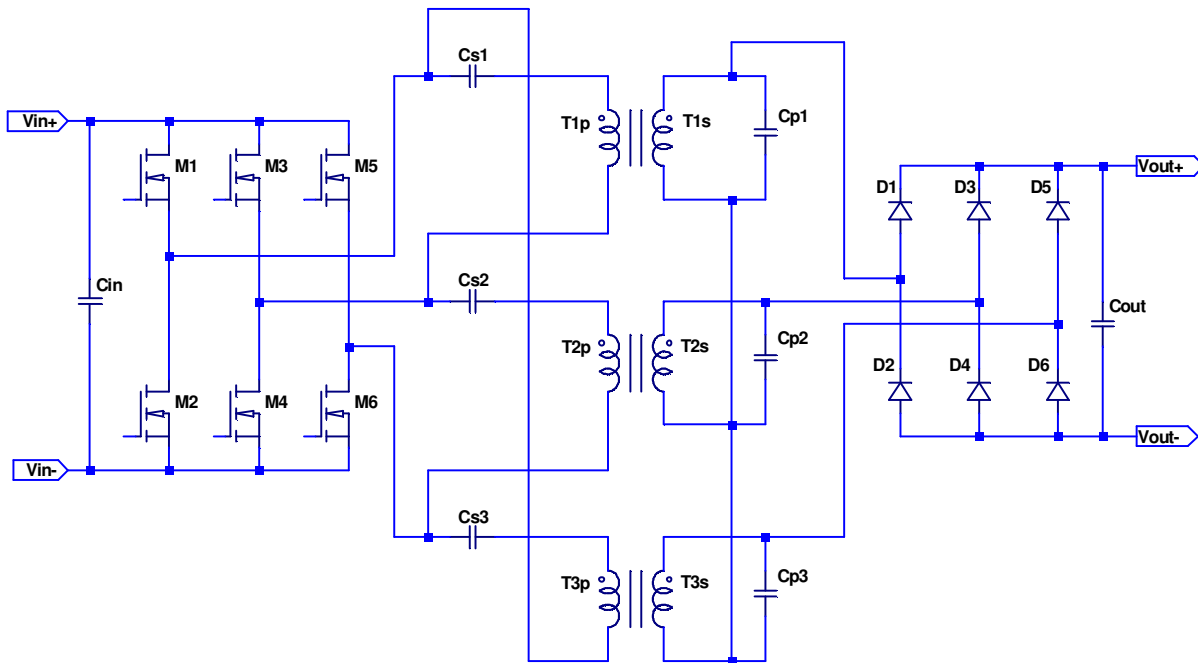


Figure 3. Standard three-phase LCC series-resonant converter.

Figure 3 is a simplified schematic diagram of a standard three-phase series resonant converter. The three-phase bridge inverter produces variable-frequency square waves. A capacitor and transformer primary winding are connected in series between each of the inverter outputs. The transformers are designed to have high leakage inductances that serve as the resonant inductances. Capacitors Cs1-Cs3 form series-resonant circuits with the transformer leakage inductances. Capacitors Cp1-Cp3 are connected in parallel with the secondary windings of the transformers. A three-phase diode bridge rectifies the output voltages supplied by the transformers. An optional output filter capacitor, Cout, is connected across the dc output terminals. The resonant converter of Figure 3 is a three-phase version of what is commonly called an LCC resonant converter.

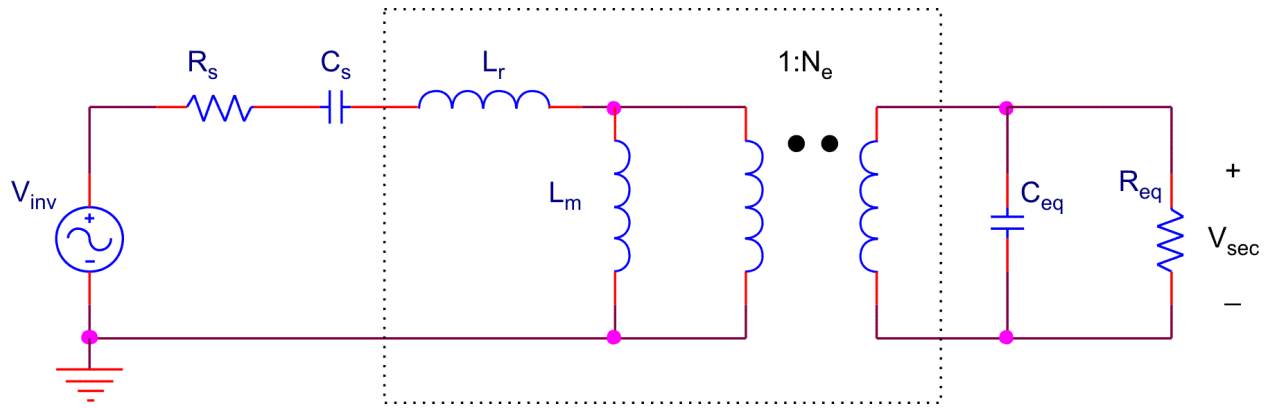


Figure 4. Simplified model of an LCC resonant circuit.

The operation of the circuit of Figure 3 can be understood by analyzing the simplified model of a single-phase LCC resonant circuit as shown in Figure 4 using a technique called the Extended Fundamental Frequency Analysis<sup>10</sup>. The ac voltage source  $V_{inv}$  represents the fundamental component of the voltage driving the series-connected capacitor and primary winding of one phase of the converter. The transformer is modeled using the resonant leakage inductance  $L_r$ , a magnetizing inductance  $L_m$ , and an ideal transformer with a turns ratio  $1:N_e$ .  $L_m$  typically has about 10 times the inductance of  $L_r$ . The losses due to the MOSFET and transformer resistances are modeled to a first-order approximation as  $R_s$ .

The power delivered by the converter is controlled by adjusting operating frequency. The control circuit maintains the operating frequency above the resonant frequency so that switching occurs before the polarity of the current flowing in the transformer primaries reverses. In other words, the load on the inverter appears inductive rather than capacitive. When a switching transistor turns off, the inductive current drives the voltage on the other switching transistor to zero before that switch is turned on. This effect is called zero voltage switching (ZVS), and is one of the main reasons for the high efficiencies obtained with resonant converters.

There are four central concepts behind the extended fundamental frequency analysis method. The first is that the current flowing through the transformer is nearly sinusoidal even though the primary and secondary voltages are not sinusoidal. The second concept is that power flow in the frequency domain is calculated through the products and phase angles of voltages and currents at the same frequency. Products of voltages and currents at different frequencies produce zero average power flow. The third concept is that the capacitors connected in parallel with the secondary windings and the diode bridge can be modeled as equivalent capacitances and resistances  $C_{eq}$  and  $R_{eq}$  which have values that depend on the dc load resistance, the operating frequency and losses in the diode bridge. The fourth concept is the basis of how  $C_{eq}$  and  $R_{eq}$  are derived and used.

Before discussing the fourth concept, it is useful to examine the simplified model of Figure 4 to get an intuitive understanding of why the circuit of Figure 3 can deliver full power over a 2:1 output voltage range. When the dc load resistance is relatively low, the impedance of  $C_{eq}$  is much higher than  $R_{eq}$ , and the circuit functions as a series-loaded series resonant circuit. When full power is being delivered to low output impedances, the operating frequency is adjusted toward the series-resonant operating frequency.

When the dc load resistance is relatively high, the impedance of  $C_{eq}$  is lower than  $R_{eq}$ , and the circuit functions as a parallel-loaded series-resonant circuit. The parallel-resonant frequency is higher than the series-resonant frequency.

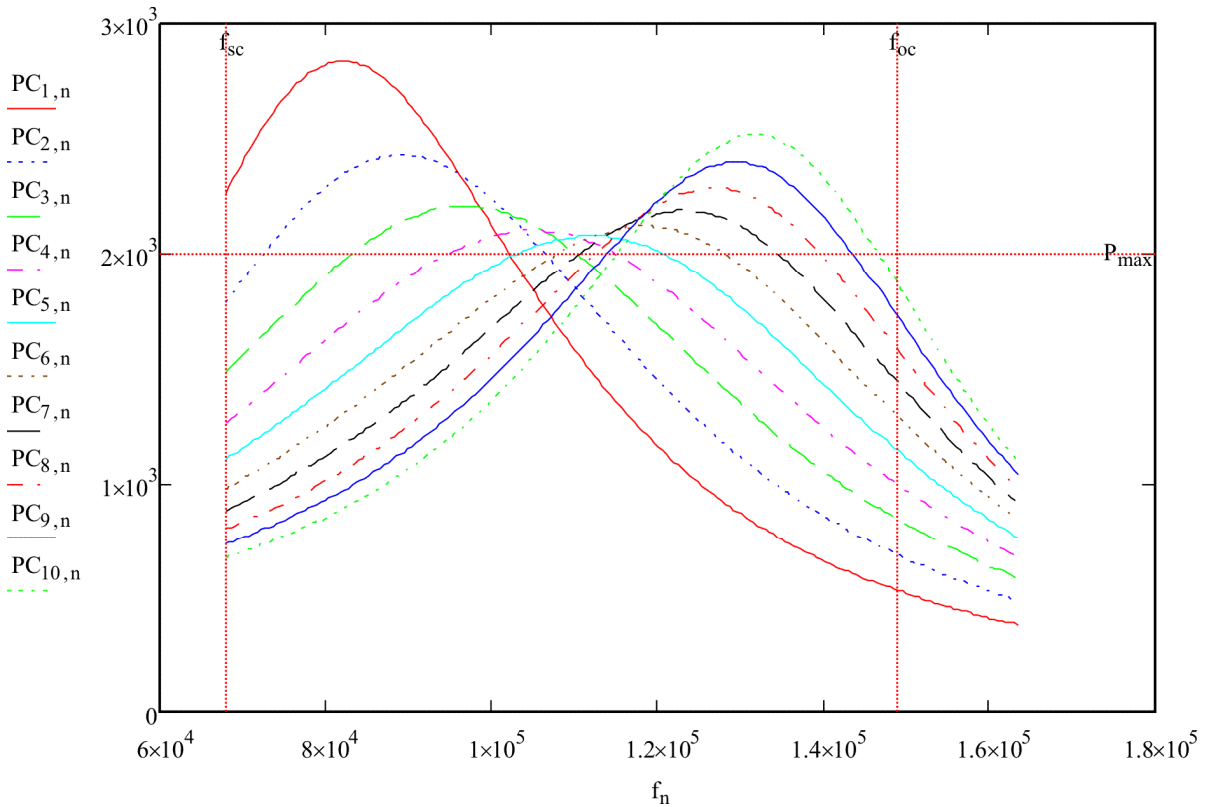


Figure 5. Output power curves of a standard LCC series-resonant converter for a set of load resistances as the operating frequency is swept.

Figure 5 shows plots of the output power for a set of load resistances as the operating frequency is varied. The maximum rated power for the converter,  $P_{max}$ , is below the locus of the peaks of the power curves. The resonant frequency for a shorted output is indicated by  $f_{sc}$ , and the resonant frequency for an open circuit load is indicated by  $f_{oc}$ . The effect of shifting between the series-resonant operating mode and the parallel-resonant operating mode is analogous to a continuously variable transmission for an engine. For an engine, it is desirable to keep the rpm in an optimal range as the driving speed is varied. For a power converter, it is desirable to keep the rms value of the switch and transformer currents relatively constant at full operating power as the load resistance and output voltage are varied. This effect is illustrated in Figure 6, in which normalized values of the primary current are plotted with respect to the output voltage of a converter that has a full-power output voltage range that varies from 800 V to 1600 V, and a dc bus input voltage that ranges from 94 V to 110 V. The plot shows that the ratio of the maximum primary current to the minimum primary current is about 1.25 over the entire range.

The fourth concept of the Extended Fundamental Frequency Analysis method relates to the fact that the transformer voltages are distorted, and that this distortion depends on the operating conditions. The authors who named this analysis method used analytical methods to derive the effective resistance and capacitance values  $R_{eq}$  and  $C_{eq}$  for particular operating conditions<sup>10</sup>. The present work was enabled by noticing that there are fixed relationships between the effective resistor and capacitor values and a quality factor value  $Q_s$  that is equal to the ratio of the dc load resistance divided by the reactance of the parallel-connected capacitors at the operating frequency.

When the converter is operating at full power and low dc output resistances, the voltage waveforms at the input of the output rectifier bridge are sine waves that have been truncated to the point that they are nearly square waves. In contrast, when the converter is operating at full power and high dc output resistances, the rectifier input voltage waveforms are nearly pure sine waves. The rectified output voltage is nearly equal to the peak value of the input waveforms. A scaling factor  $k_{rect}$  is equal to the ratio

of the rectified dc output voltage divided by the peak value of the fundamental component of the voltage waveform across one of the transformer secondary windings. In Figure 7,  $k_{\text{rect}}$  is plotted with respect to  $Q_S$ . The  $k_{\text{rect}}$  values were derived through a series of SPICE simulations. It conveniently turns out that the relationship between  $k_{\text{rect}}$  and  $Q_S$  is independent of the load resistance and parallel capacitance. Once this relationship has been documented from one set of simulations, an interpolated function for design purposes can be created from the data, and the function can be used as part of a synthesis tool for designing this type of converter.

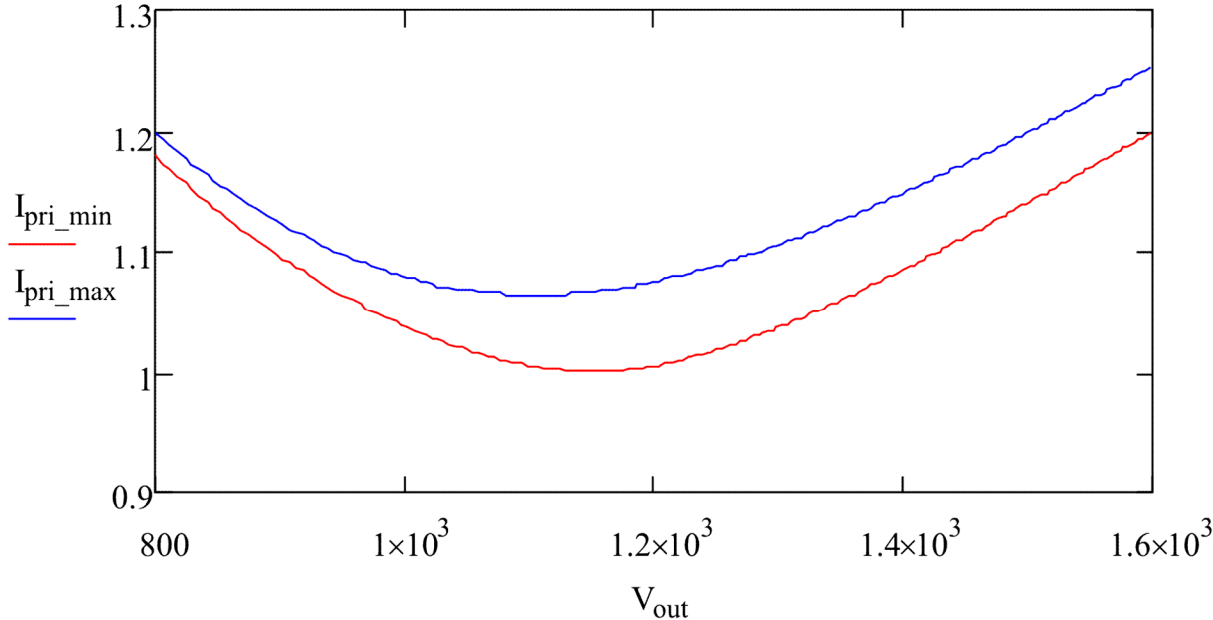


Figure 6. Full-load rms primary currents of a standard LCC series-resonant converter as the output voltage is varied, for minimum and maximum dc input voltages.

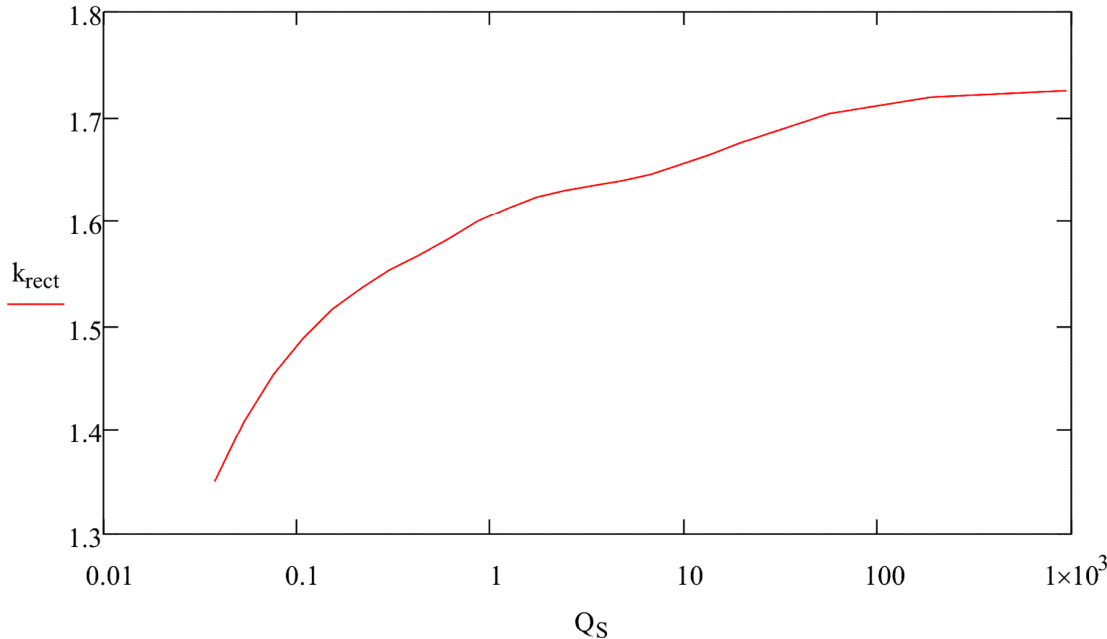


Figure 7. Rectifier scaling factor  $k_{\text{rect}}$  as a function of  $Q_S$  for a standard LCC series-resonant converter.

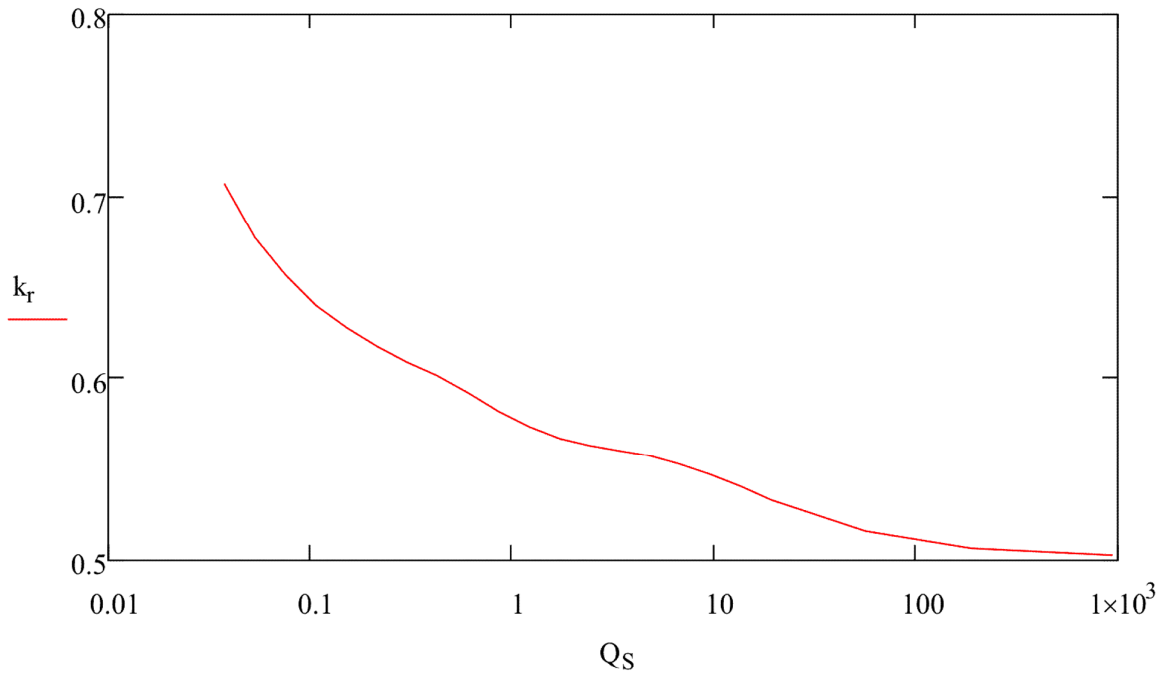


Figure 8. Resistor scaling factor  $k_r$  as a function of  $Q_s$  for a standard LCC series-resonant converter.

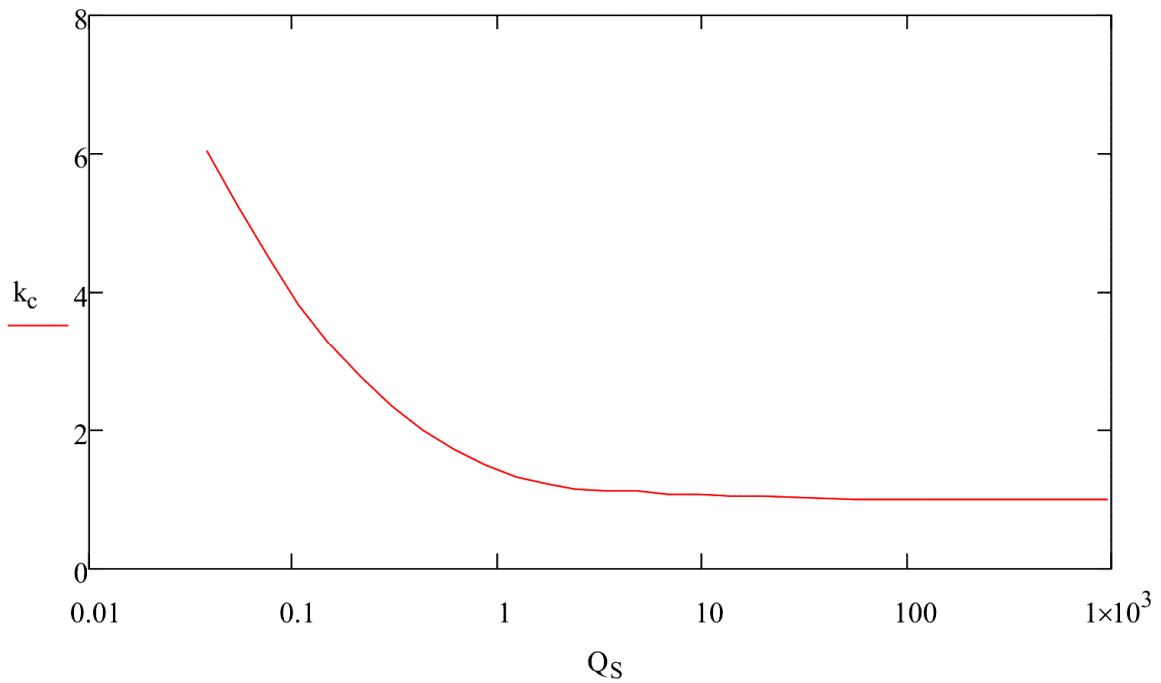


Figure 9. Capacitor scaling factor  $k_c$  as a function of  $Q_s$  for a standard LCC series-resonant converter.

The effective resistance and capacitance values  $R_{eq}$  and  $C_{eq}$  can be determined for a particular operating condition by multiplying the dc load resistance with a scaling factor  $k_r$ , and by multiplying the capacitance connected in parallel with the transformer secondary windings with a scaling factor  $k_c$ . Plots of  $k_r$  and  $k_c$  with respect to  $Q_s$  are shown in Figures 8 and 9.

The values of  $k_r$  and  $k_c$  were derived from examining the phase angle between the transformer secondary voltage and current, the diode losses and the delivered output power. This information was derived from the same set of simulations that were used to determine  $k_{rect}$ . Fortunately, SPICE has provisions for automatically running a set of simulations with varying component values using the .STEP command, and can automatically take and tabulate measurements using the .MEAS command.

### WIDE-RANGE THREE-PHASE LCC SERIES-RESONANT CONVERTER

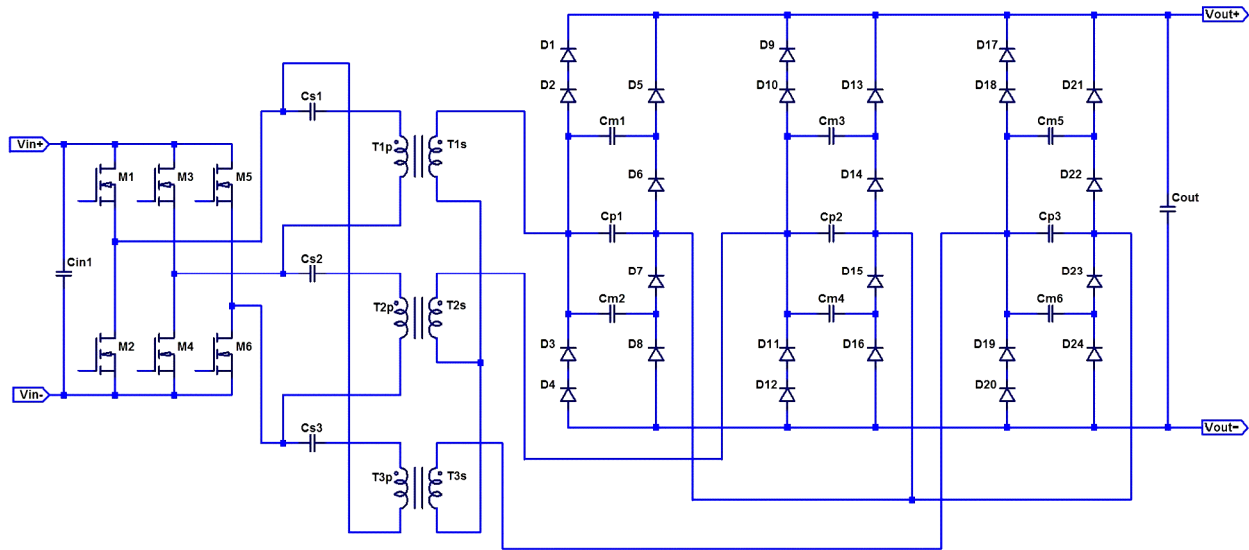


Figure 10. Wide-range three-phase LCC series-resonant converter.

Figure 10 is a simplified schematic diagram of a wide-range three-phase LCC series-resonant converter. The differences between this circuit and the standard circuit of Figure 3 are what is connected to the transformer secondary windings. Capacitors Cp1-Cp3 serve the same parallel-resonant function as capacitors Cp1-Cp3 in Figure 3. The rectifier bridge is actually a set of voltage multipliers. The capacitors with designators starting with Cm are the multiplier capacitors. Each multiplier stage is bypassed by a pair of diodes such as D1 and D2. When output current is relatively high, the output current is primarily delivered through the bypass diodes. When the output current is relatively low, the output current is delivered through the multiplier diodes. For moderate output currents, the output current is delivered through bypass diodes and the multiplier diodes. Returning to our previous engine transmission analogy, the transition between the operating modes is like adding an additional “gear ratio” to the two “gear ratios” provided by the series-resonant and parallel-resonant operating modes. The new rectifier circuit allows full-power operation over a 5:1 output voltage range. CPE has developed a variety of new rectifier circuits that have characteristics that are useful for various applications, but the details are beyond the scope of this paper.

Similar to Figure 5, Figure 11 shows plots of the output power of a wide-range LCC series-resonant converter for a set of load resistances as the operating frequency is varied. The maximum rated power for the converter,  $P_{max}$ , is below the locus of the peaks of the power curves. The resonant frequency for a shorted output is indicated by  $f_{sc}$ , and the resonant frequency for an open circuit load is indicated by  $f_{oc}$ .

Similar to Figure 6, Figure 12 shows normalized values of the primary current are plotted with respect to the output voltage of a converter that has a full-power output voltage range that varies from 200 V to 1000 V, and a dc bus input voltage that ranges from 94 V to 120 V. The plot shows that the ratio of the maximum primary current to the minimum primary current is only about 1.17 over the entire range.



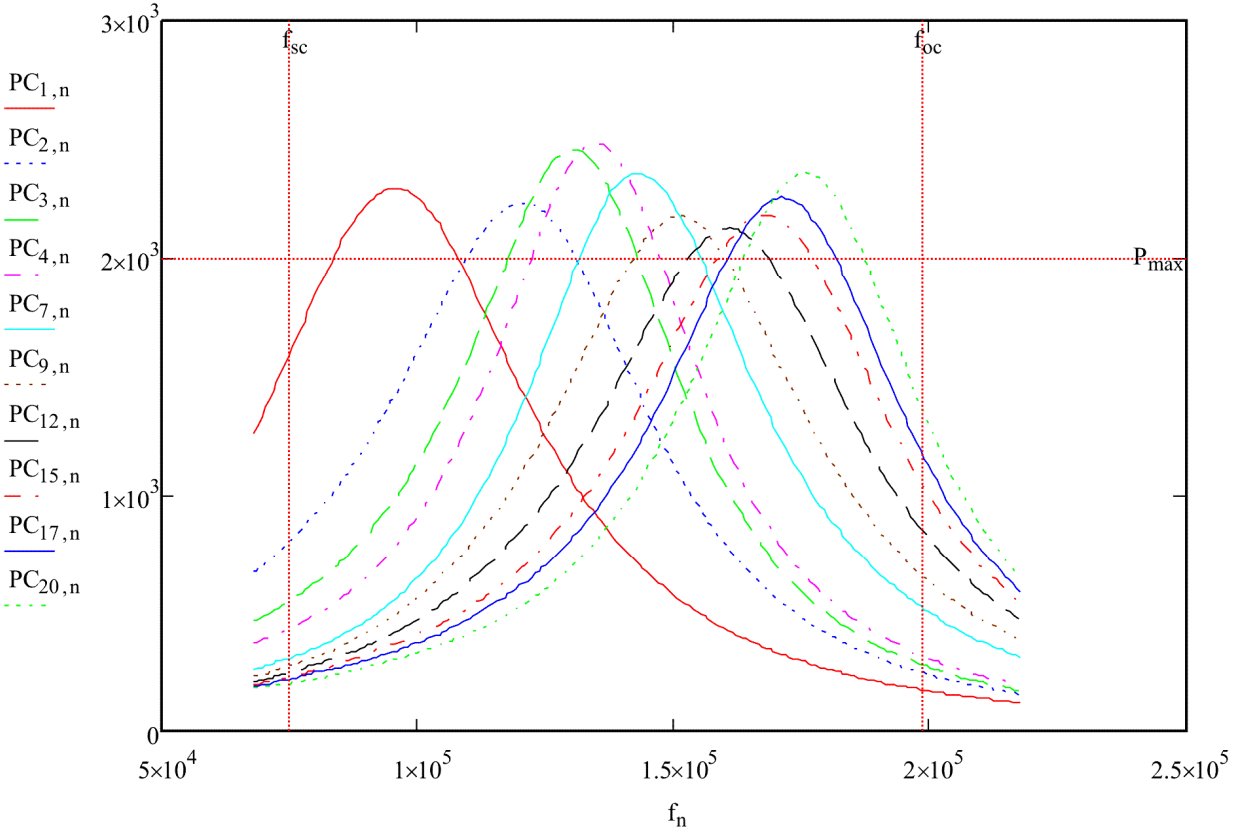


Figure 11. Output power curves of a wide-range LCC series-resonant converter for a set of load resistances as the operating frequency is swept.

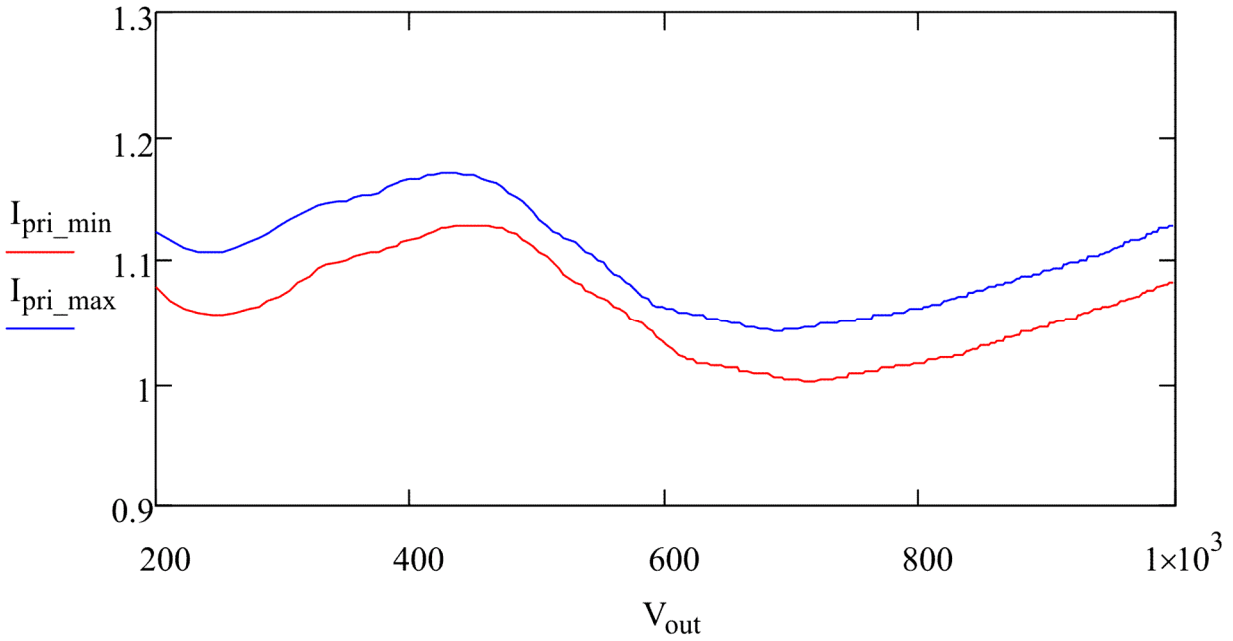


Figure 12. Full-load rms primary currents of a wide-range LCC series-resonant converter as the output voltage is varied, for minimum and maximum dc input voltages.

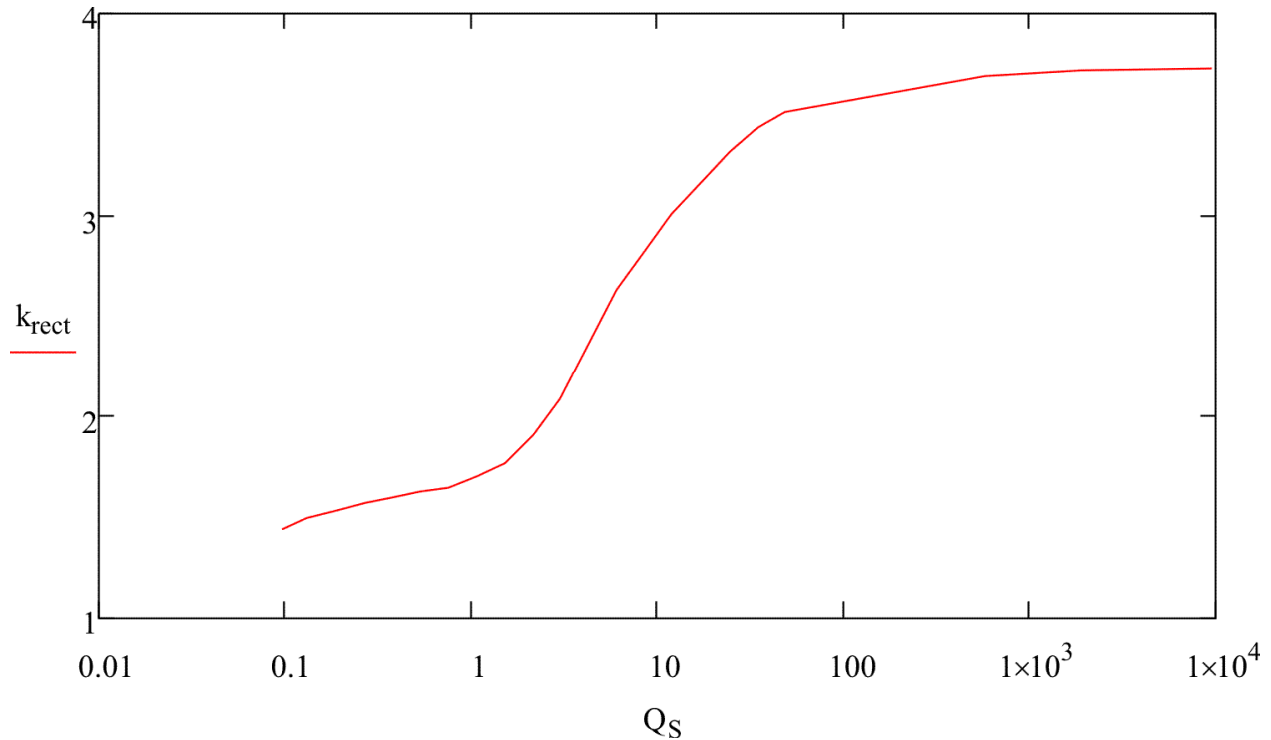


Figure 13. Rectifier scaling factor  $k_{\text{rect}}$  as a function of  $Q_S$  for a wide-range LCC series-resonant converter.

As with the standard resonant circuit, the value of quality factor  $Q_S$  for the wide range circuit was defined as the ratio of the dc load resistance divided by the reactance of the parallel-connected capacitors at the operating frequency. However, the effective parallel capacitance for the wide range rectifier circuit depends on two capacitor types, the parallel capacitors and the multiplier capacitors. Consequently, the scaling factor curves are only valid for a given ratio of the parallel capacitance to the multiplier capacitance. In this case, the value of the multiplier capacitors was twice the value of the parallel capacitors.

Similar to Figure 7, the rectifier scaling factor for a wide-range LCC series-resonant converter is shown in Figure 13. The maximum value of  $k_{\text{rect}}$  is 3.72 in comparison to 1.73 for the standard resonant LCC converter.

Similar to Figure 8, Figure 14 shows the resistor scaling factor  $k_r$  as a function of  $Q_S$  for a wide-range LCC series-resonant converter. Similar to Figure 9, Figure 15 shows the capacitor scaling factor  $k_c$  as a function of  $Q_S$  for a wide-range LCC series-resonant converter.

Resonant converters typically have high open-loop dc incremental output impedances, and this is beneficial for operating plasma loads such as ion engines and Hall thrusters because it helps improve the stability. Plots of the ratio of the incremental dc output impedance relative to the dc load resistance for the standard and wide range LCC resonant converters are shown in Figures 16 and 17. The ratio of the incremental dc output impedance relative to the load resistance decreases at low output power levels. Wide-range resonant converters typically have higher open-loop dc incremental output impedances than standard resonant converters.

The static analysis technique presented here can be extended to a frequency-domain small-signal gain and impedance analysis<sup>11</sup>, but that is beyond the scope of this paper.

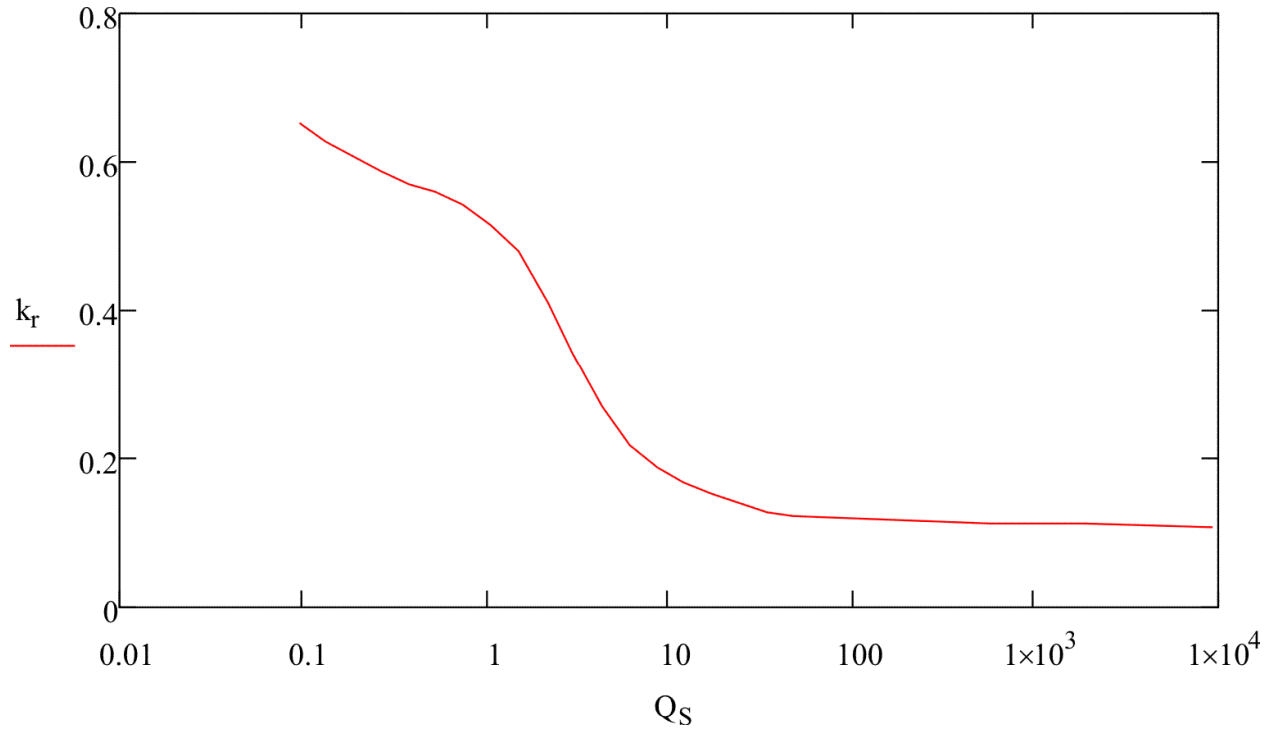


Figure 14. Resistor scaling factor  $k_r$  as a function of  $Q_s$  for a wide-range LCC series-resonant converter.

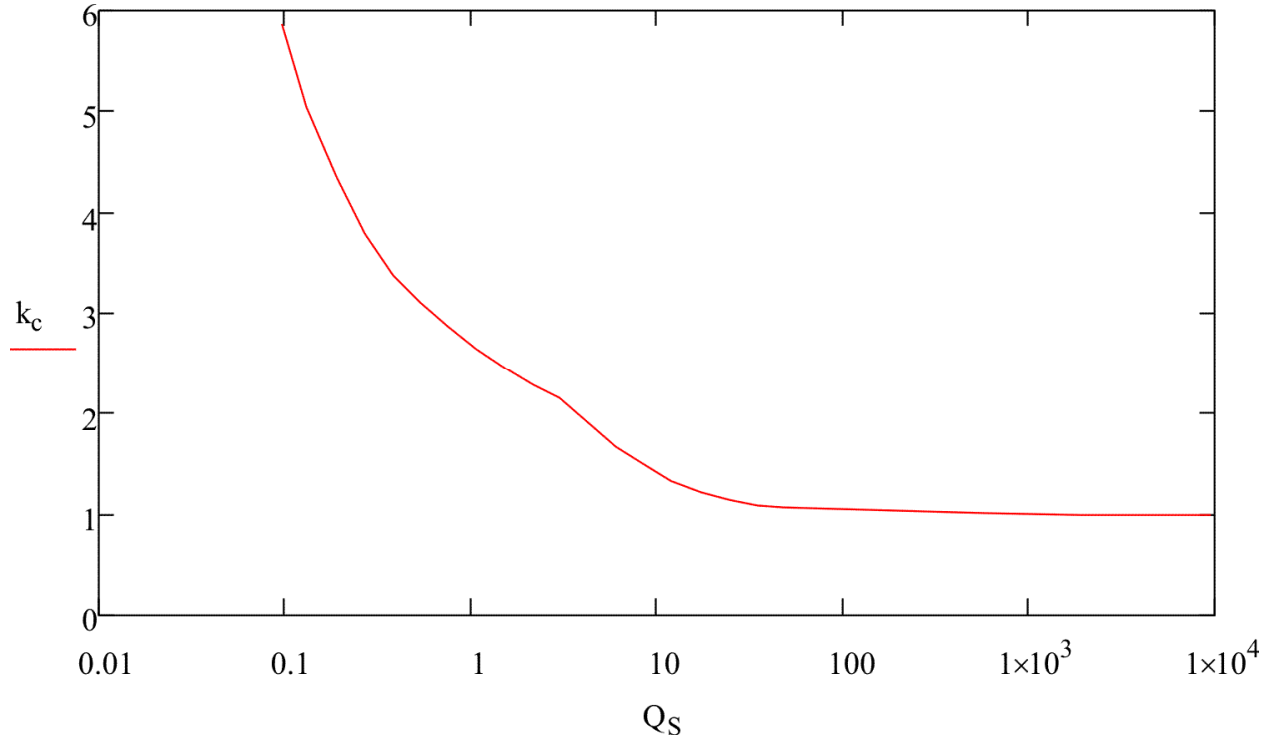


Figure 15. Capacitor scaling factor  $k_c$  as a function of  $Q_s$  for a wide-range LCC series-resonant converter.

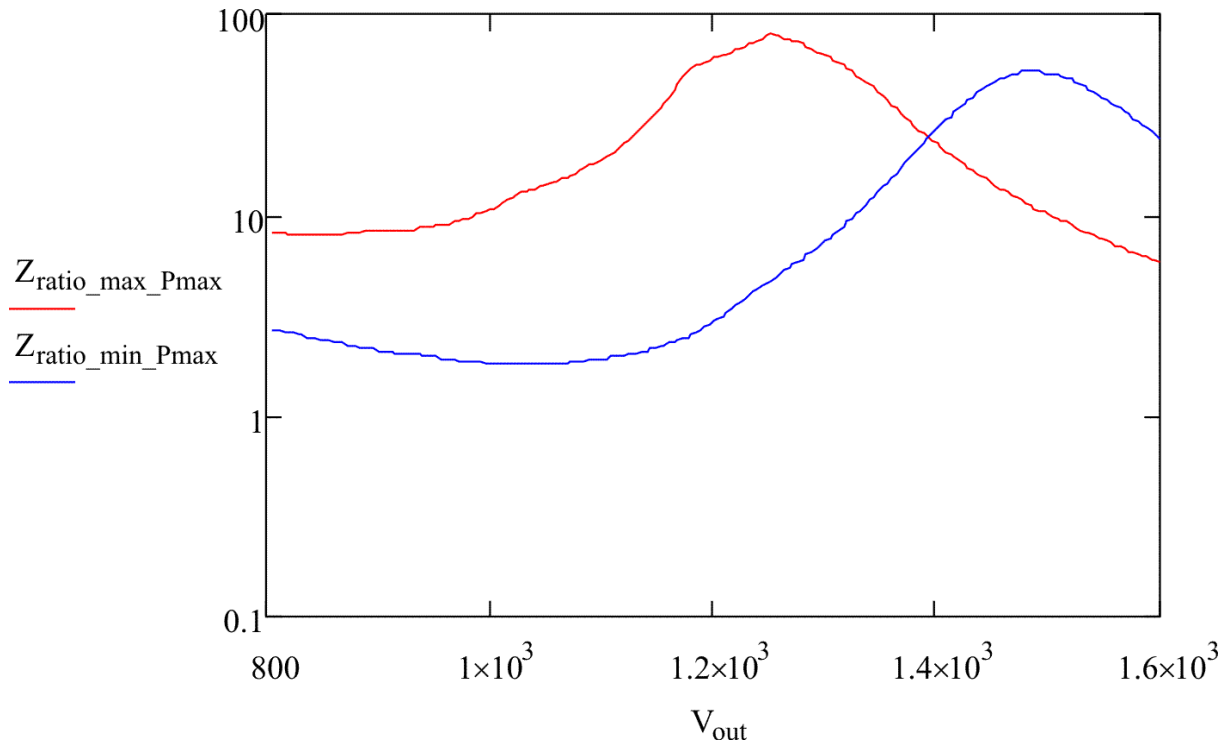


Fig. 16. Open-loop ratio of incremental output impedance to load resistance for a standard 3-phase resonant converter at full operating power with maximum and minimum bus voltages.

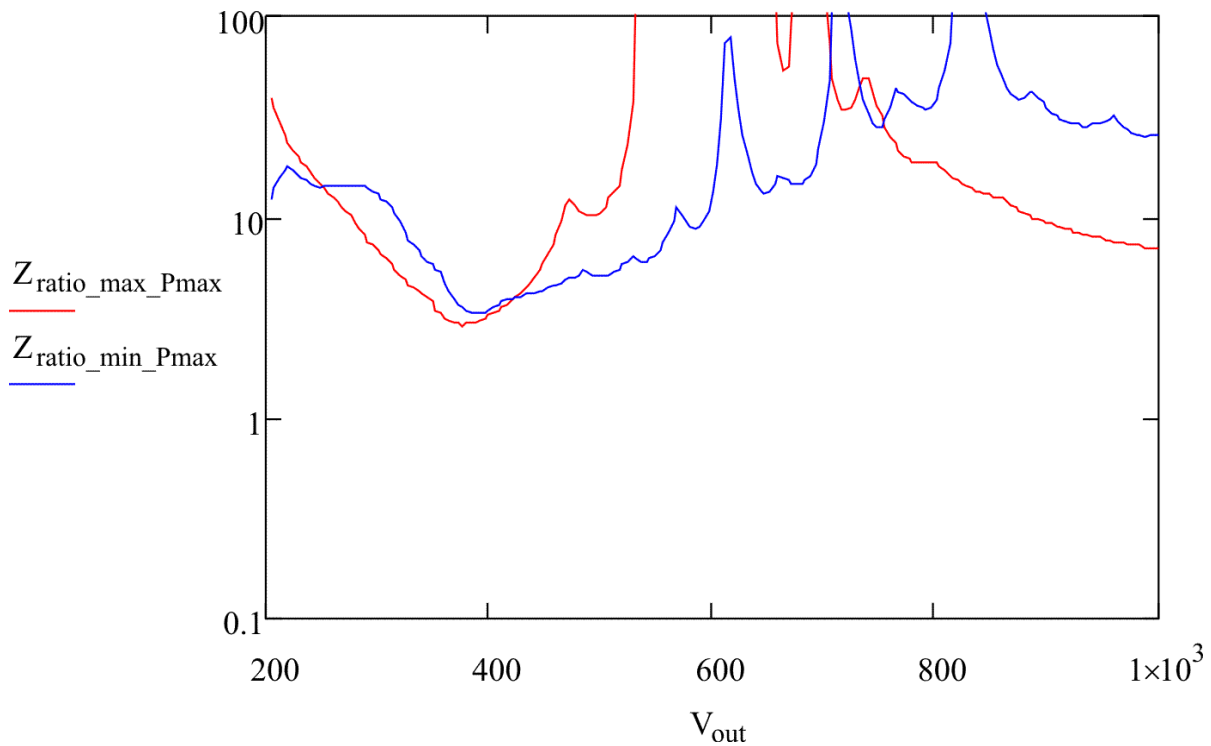


Fig. 17. Open-loop ratio of incremental output impedance to load resistance for a wide-range 3-phase resonant converter at full operating power with maximum and minimum bus voltages.

## SINGLE EVENT EFFECTS

One of the advantages of the CPE resonant converters is that the voltages seen by the switching MOSFETs are limited to the dc bus voltage. Keeping the switch operating voltage below a critical voltage,  $V_{crit}$ , greatly improves robustness to single-event effects. Parts rated at 130 V or less have  $V_{crit}$  values much closer to the rated breakdown voltage<sup>12</sup>. Because  $R_{dson}$  increases by the square of the rated voltage, while derating factors decrease with increasing rated voltage, there is a diminishing return for using parts rated beyond 130 Volts. CPE typically uses 250 V rated parts for steady-state bus voltages up to 120 V (160 V transient). One early study reported satellite power supplies with switching MOSFETs having 94536 device days in space without failure in which there was a 70V stress on 100V parts<sup>13</sup>.

CPE typically uses output rectifier diodes rated at a maximum of 600 V, and single-event breakdown is usually not a problem for diodes rated at about 1000 V or less<sup>14</sup>.

In addition to derating the voltage stress, limiting available current to less than 2 A may prevent single-event failures<sup>15</sup>, but that is impractical for high-power units. Series impedance may help prevent failures for prompt radiation, but probably not for natural radiation except at low power levels. The benefit of the series impedance due to transformer leakage inductances in push-pull circuits, however, is doubtful<sup>3</sup>. In CPE resonant converters, the low input ripple currents allow the use of small bus capacitors, and this may help prompt radiation survivability.

Regenerative feedback following particle strikes can occur in less than 1ns<sup>16</sup>, so turn-off circuits are probably too slow to prevent damage from this radiation. It is better to keep voltage stress below  $V_{crit}$ , so that regenerative feedback is unlikely to occur. If a MOSFET failure does occur, however, current sensing circuits can be used to prevent series-connected MOSFETs from failing and shorting the bus.

## **SUMMARY AND CONCLUSIONS**

Standard and wide range multiphase resonant power converters show promise of becoming preferred topologies for electric propulsion and other high-power space applications due to their high efficiency, low mass and ruggedness.

## **FUTURE WORK**

CPE is continuing progress toward producing a flightworthy PPU, and has received a phase 1 SBIR contract for 2010.

## **ACKNOWLEDGMENTS**

This work is supported in part by a NASA SBIR projects administered by the NASA Glenn Research Center. The support and the advice provided by NASA engineers Luis Piñero and Hani Kamhawi are gratefully acknowledged. Geoff Drummond was the principle investigator for the initial NASA projects, and I appreciate the opportunity that he has given me to take a leading role in moving this technology toward commercialization. Dr. John D. Williams of Colorado State University provided valuable consulting services. My appreciation is expressed to Eric Scheel, and Derek Krise for their careful craftsmanship in fabricating the PPU prototypes, and to Teresa Drummond for her administrative support.

## **REFERENCES**

1. Jackson, W. E. and Thibodeaux, R., ***Space Power Converter Selection Methodologies***, Proceedings of the 25th Intersociety Energy Conversion Engineering Conference, IECEC-90, 1990, pp. 26-29.

2. Kay, R, Edwards, D., Kristalinski, A. and McCrea, B., **Summary Evaluation of Power Processor Topologies**, Space Power Workshop 2006, Manhattan Beach, CA (April 25-27, 2006).
3. Drummond, G. N. and Williams, J. D., **Ion and Plasma Thruster Test Console Based on Three-Phase Resonant Conversion Power Modules**, AIAA 2006-4339, 42nd AIAA/ASME/SAE/ASEE Joint Propulsion Conference & Exhibit, Sacramento, Calif., (July 9-12, 2006), pp. 1-17.
4. Drummond, G. N., **Advanced Power Converters for Spacecraft Applications**, Space Power Workshop 2006, Manhattan Beach, CA (April 25-27, 2006).
5. Drummond, G. N., and Hesterman, B. L., US Patent 6,697,265, **Wide range DC power supply utilizing voltage doubling output capacitors and inductive choke to extend full power load impedance range**, (February 24, 2004).
6. Drummond, G. N., and Hesterman, B. L., US Patent Application 12/586,985, **Wide range DC power supply with bypassed multiplier circuits**, (September 30, 2009).
7. Kamhawi, H., Manzella, D., Piñero, L. R. and Haag, T., **In-Space Propulsion High Voltage Hall Accelerator Development Project Overview**, AIAA 2009-5282, 45th AIAA Joint Propulsion Conference, Denver, Colorado (August 2-5, 2009).
8. Piñero L. R., Kamhawi, H. and Drummond, G. N., **Integration Testing of a Modular Accelerator Development Project Discharge Supply for NASA's High Voltage Hall Accelerator Thruster**, IEPC-2009-275, 31st International Electric Propulsion Conference, Ann Arbor, Michigan, (September 20-24, 2009).
9. Drummond G. N. and Monheiser, J. M., US Patent 7,631,482, **Multi-Phase Power Supply for Rocket Engines**, (December 15, 2009).
10. Forsyth, A. J., Ward, G. A. and Mollov, S. V., **Extended Fundamental Frequency Analysis of the LCC Resonant Converter**, IEEE Trans. on Power Electronics, Vol. 18, No. 6, (NOVEMBER 2003) pp. 1286-1292.
11. van Zyl, G. J. J., **A Novel Frequency-Domain Small-Signal Analysis of Resonant Power Converters**, IEEE Trans. on Circuits and Systems—I: Regular Papers, vol. 51, No. 7, (July 2004), pp. 1379-1384.
12. Scheick, L. and Selva, L. **Sensitivity to LET and Test Conditions for SEE Testing of Power MOSFETs**, IEEE Radiation Effects Data Workshop, (2009) pp. 82-93.
13. Brucker, G.J., Measel, P., Oberg, D., Wert, J. and Criswell, T. **SEU Sensitivity of Power Converters**, IEEE Trans. on Nuclear Science, Vol. NS-34, No. 6, (December 1987), pp. 1792-1795.
14. Foutz, J., **Power Transistor Single Event Burnout**, <http://www.smpstech.com/power-mosfet-single-event-burnout.htm>
15. Tastet, P., Garnier, J., Constans, H. and Tizon, A. H., **Burnout sensitivity of power MOSFETs operating in a switching converter**, IEEE Transactions on Nuclear Science Vol. 41. No. 3, (June 1994), pp. 583-588.
16. Johnson, G. H., Brews, J. R., Schrimpf, R. D. and Galloway, K. F., **Analysis of the time-dependent turn-on mechanism for single-event burnout of n-channel power MOSFETs**, Second European Conference on Radiation and its Effects on Components and Systems, RADECS 93, (1993), pp. 441-445.